



# Low friction of graphene nanocrystallite embedded carbon nitride coatings prepared with MCECR plasma sputtering

Pengfei Wang<sup>a</sup>, Weiqiang Zhang<sup>b</sup>, Dongfeng Diao<sup>a,\*</sup>

<sup>a</sup> Institute of Nanosurface Science and Engineering, Guangdong Provincial Key Laboratory of Micro/Nano Optomechatronics Engineering, Shenzhen University, Shenzhen 518060, China

<sup>b</sup> Key Laboratory of Education Ministry for Modern Design and Rotor-Bearing System, School of Mechanical Engineering, Xi'an Jiaotong University, Xi'an 710049, China

## ARTICLE INFO

### Keywords:

Carbon nitride  
Graphene nanocrystallite  
Low friction  
Tribofilm

## ABSTRACT

Graphene nanocrystallite embedded carbon nitride (GNECN) coatings were fabricated with the mirror confinement electron cyclotron resonance (MCECR) plasma sputtering system under low energy electron irradiation at various N<sub>2</sub>/Ar ratios. N<sub>2</sub>/Ar ratio was clarified to be an effective deposition parameter for tailoring the composition and structure of the GNECN coatings. It was observed that the deposition rate, N/C atomic ratio, internal stress, surface roughness, and scratch depth of the prepared GNECN coatings change greatly with the increasing N<sub>2</sub>/Ar ratio from 1/11 to 1/3. Graphene nanocrystallite was clearly identified in the amorphous carbon nitride structure from the analyses of TEM, XPS, and Raman spectroscopy. Moreover, the friction behavior of the GNECN coatings sliding against Si<sub>3</sub>N<sub>4</sub> balls in both ambient air and N<sub>2</sub> gas stream showed less dependency on the N<sub>2</sub>/Ar ratio. Specifically, high friction coefficients ranging from 0.10 to 0.15 were obtained in ambient air, whereas, stable and low friction coefficients of < 0.05 were achieved in N<sub>2</sub> gas stream. Optical images and Raman spectra of the worn surfaces on the Si<sub>3</sub>N<sub>4</sub> balls and GNECN coatings suggested that a homogeneous tribofilm on the mating ball surface together with the generation and evolution of the nano-size graphene structure in the GNECN coating are the key points in achieving stable and low friction coefficients of < 0.05 of the GNECN coatings in N<sub>2</sub> gas stream. Finally, it was argued that the combination of low energy electron irradiation and nitrogen atom incorporation in the MCECR plasma sputtering system results in the embedding of soft graphene nanocrystallites into hard carbon nitride matrix, providing a beneficial architecture for achieving stable and low friction coefficients of GNECN coatings in N<sub>2</sub> gas stream.

## 1. Introduction

Carbon nitride coatings have drawn numerous attentions in the last two decades since the prediction of crystalline β-C<sub>3</sub>N<sub>4</sub> structure with a bulk modulus and hardness comparable or even superior to that of diamond [1]. Tremendous efforts have been devoted to the synthesis of carbon nitride coatings with various types of deposition techniques, such as direct current magnetron sputtering (DCMS) [2,3], high power impulse magnetron sputtering (HiPIMS) [4], plasma enhanced chemical vapor deposition (PECVD) [5], femtosecond pulsed laser deposition (fs-PLD) [6], and ion beam assisted deposition (IBAD) [7,8].

To date, the so obtained carbon nitride coatings are amorphous mixtures of carbon and carbon nitride phases together with a maximum nitrogen atomic concentration of less than the theoretical value of 57 at.% [9,10]. However, amorphous carbon nitride coatings with a desirable combination of mechanical (high hardness) and tribological properties (low friction coefficient and high wear resistance) have made

them good candidates as hard- and wear- protective coatings in demanding tribological applications [11–15]. Moreover, the formation of local layered or crystalline structures in the amorphous carbon nitride coatings could tailor the mechanical, chemical, electrical, and even optical properties of the coatings, e.g. fullerene-like structure could improve the resiliency, friction, and wear behavior of fullerene-like carbon nitride coatings (FL-CN<sub>x</sub>) [4,16,17], graphitic layered structure could improve the catalytic and optoelectronic properties of graphitic carbon nitride coatings (g-CN or g-C<sub>3</sub>N<sub>4</sub>) [18,19].

Recently, graphene materials have attracted considerable interest in advanced tribological fields due to their outstanding performances in reducing friction and wear of contact materials from nanoscale to microscale [20–26]. According to our previous research, the graphene sheets are incorporated into amorphous carbon structure thanks to the customized electron cyclotron resonance (ECR) sputtering system, which is beneficial for achieving stable and low friction coefficients of amorphous carbon coatings when running against Si<sub>3</sub>N<sub>4</sub> balls in

\* Corresponding author.

E-mail address: [dfdiao@szu.edu.cn](mailto:dfdiao@szu.edu.cn) (D. Diao).

**Table 1**  
Deposition conditions of GNECN coatings.

Deposition parameters	Value
Working pressure (Pa)	0.04
N <sub>2</sub> gas flow ratio (sccm)	0.3, 0.4, 0.6, 0.9
Ar gas flow ratio (sccm)	3.3, 3.2, 3.0, 2.7
Microwave power (W)	500
Target bias voltage (V)	-500
Substrate bias voltage (V)	+20

ambient air [27,28]. Therefore, in this study, amorphous carbon nitride coatings with embedded graphene nanocrystallites are fabricated using the ECR sputtering system with the objective to achieve stable and low friction coefficients of the amorphous carbon nitride coatings. Furthermore, the low friction mechanism of the amorphous carbon nitride coatings will be discussed from the viewpoint of composition and structural changes on the worn surfaces.

## 2. Experimental details

### 2.1. Coating deposition

Graphene nanocrystallite embedded carbon nitride (GNECN) coating in this study was deposited onto a p-type 100-oriented single crystal silicon substrate (thickness of  $525 \pm 25 \mu\text{m}$ ) by utilizing a customized mirror confinement electron cyclotron resonance (MCECR) plasma sputtering system, in which the low energy electron irradiation technique was introduced to facilitate the formation of graphene nanocrystallites in the coating [29–32]. Table 1 shows the deposition conditions of GNECN coatings. Specifically, MCECR plasma was generated when a 2.45 GHz microwave with a power of 500 W was employed and a magnetic field was applied to the vacuum chamber. Before deposition, the vacuum chamber was first evacuated to a background pressure of  $< 1.0 \times 10^{-4}$  Pa using an air cooled dry pump (Neo-Dry15E, Kashiyama) and a compound molecular pump (TG450FVAB, Osaka Vacuum), and then a working pressure of  $4 \times 10^{-2}$  Pa was controlled in the following process. The silicon substrate was treated with argon plasma sputtering for 3 min under a DC bias voltage of  $-50$  V in order to eliminate the native oxide layer on the silicon surface. Afterwards, the carbon target was sputter-cleaned for 3 min to achieve a stable target bias voltage of  $-500$  V. Subsequently, the deposition of GNECN coating was carried out in a flowing mixed gas of argon and nitrogen gas atmosphere. The N<sub>2</sub>/Ar ratios of gas mixture used in the experiment were 1/11 (0.3 sccm and 3.3 sccm), 1/8 (0.4 sccm and 3.2 sccm), 1/5 (0.6 sccm and 3.0 sccm), and 1/3 (0.9 sccm and 2.7 sccm), respectively. Particularly, 1/11 was the minimum value of the N<sub>2</sub>/Ar ratio according to the equipment limitation. Whereas, 1/3 was the maximum value of the N<sub>2</sub>/Ar ratio, beyond which a strong reaction between nitrogen gas molecules and carbon atoms occurred (i.e. re-sputtering or etching effect) and caused an extremely low deposition rate of the coatings. A positive DC substrate bias voltage of  $+20$  V was applied during the deposition to realize a low energy electron irradiation on the substrate. Two series of GNECN coatings were prepared in this study; one was deposited for 30 min to standardize the deposition rate and the other was deposited to a thickness of approximately 200 nm to prevent potential thickness effect on the structural and tribological performances of the GNECN coatings.

### 2.2. Coating characterization

A surface profilometer (Dektak-XT, Bruker) was used to measure the thickness of the as-deposited GNECN coatings with the introduction of a step formed by a shadow mask. The deposition rate of GNECN coating was directly calculated from the coating thickness. The residual stress was calculated according to the Stoney equation based on the

traditional bending beam method, in which the central deformation was measured from the surface profilometer [33–35]. The surface morphologies and scratch behaviors of the GNECN coatings were evaluated by an atomic force microscope (AFM, Dimension Edge, Bruker) under peak force tapping mode and contact mode with a scan area of  $5 \mu\text{m} \times 5 \mu\text{m}$ , respectively. In case of surface morphology, a probe (SCANASYST-Air, Bruker) with a tip radius of 2 nm was employed to derive the arithmetic mean surface roughness (Ra) of the coating. Whereas, for the scratch behavior, a probe (DNISP, Bruker) with a diamond tip and tip radius of 40 nm was applied to scratch the specimen three times at a normal load of 120  $\mu\text{N}$  and scratch length of 2  $\mu\text{m}$ , and then the cross-sectional topographies of the scratch tracks were examined to calculate the average scratch depths, which represents the nano-scratch resistance of the coatings.

The featured microstructures of the as-prepared GNECN coatings were investigated on a high resolution transmission electron microscope (HRTEM, Tecnai G<sup>2</sup> F30, FEI) at an accelerating voltage of 300 kV with a point-to-point resolution of 0.205 nm. TEM specimen for the plan view was prepared by scratching the coating surface with a diamond tip pen and collecting the delaminated flakes onto a copper microscope grid. The chemical composition and bonding configuration of GNECN coatings were analyzed using an X-ray photoelectron spectroscope (XPS, Axis Ultra DLD, Kratos) with a monochromatic Al K $\alpha$  (photo energy of 1486.6 eV) X-ray source. The relative atomic concentrations of carbon, nitrogen, and oxygen elements in GNECN coatings were determined taking into account the atomic sensitivity factors and area ratios of the C1s, N1s, and O1s peaks in XPS spectra of the coatings. The bonding structure information of the GNECN coating was also obtained via a Raman spectroscope (LabRAM HR Evolution, Horiba) with a 532 nm Ar-ion laser as the excitation source at a detecting range from 800 to 3500  $\text{cm}^{-1}$ . Laser power was chosen carefully to avoid any possible heating damage on the specimen surface.

### 2.3. Tribological characterization

Frictional behavior of GNECN coatings were evaluated using a home-built ball-on-disk apparatus which consisted of a rotating disk sliding against a stationary ball at room temperature with a relative humidity of 50–60%RH. Friction tests were carried out both in ambient air as well as in nitrogen gas stream, where dry nitrogen gas was blown to the contact interface with a gas tube (diameter of 6.35 mm) under a fixed gas flow rate of 2.0 L/min. The relative humidity around the contact point of the sliding interface is  $< 5\%$ RH. This kind of nitrogen gas supply technique has been adopted by several researchers to carry out friction test in dry N<sub>2</sub> gas environment [12,13,15,34]. The GNECN coating deposited on silicon substrate with dimensions of 25 mm  $\times$  25 mm was mounted on a glass plate using a double sided tape and placed in sliding contact against a counterface made of 6.35 mm diameter Si<sub>3</sub>N<sub>4</sub> ball (Ra of 50 nm) on which a normal load of 1.0 N was applied (corresponding to a maximum contact Hertzian pressure of approximately 650 MPa). The wear track diameter on the disk was set to 3 mm, which corresponded to a sliding velocity of 28.3 mm/s at fixed rotary speed of 180 rpm. Each friction test ran for 5000 cycles. The normal load and frictional force exerted on the ball were continuously detected by two sets of strain gauges (KFG-5-120-C1-16, Kyowa). The strain gauge output voltage was measured by a strain amplifier (DPM-951A, Kyowa) and recorded by a data collecting system (NR-500, Keyence) via a personal computer with a sampling frequency of 5 Hz. The worn surfaces on the Si<sub>3</sub>N<sub>4</sub> balls and the GNECN coatings were observed with an optical microscope (LV-150N, Nikon) as well as with a Raman spectroscope.

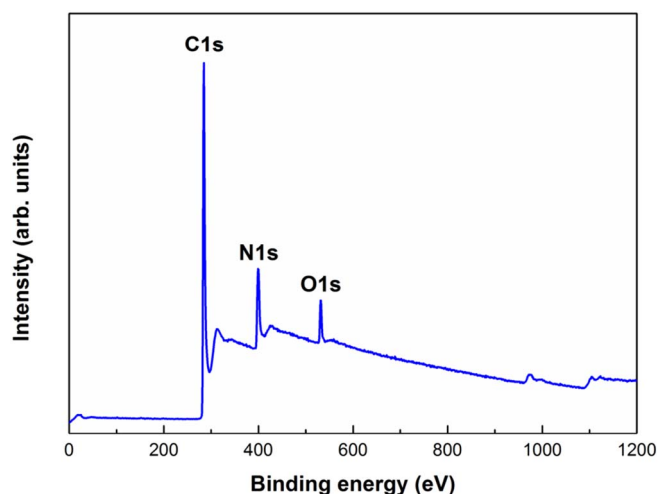


Fig. 1. A typical XPS wide scan spectrum of GNECN coating prepared at  $N_2/Ar$  ratio of 1/11.

### 3. Results and discussion

#### 3.1. Composition and structure of GNECN coatings

Fig. 1 shows a typical XPS wide scan spectrum of GNECN coating prepared at  $N_2/Ar$  ratio of 1/11. The presence of nitrogen peak (N1s) in the spectrum clearly implied that nitrogen atom is successfully incorporated into carbon structure. Additionally, the presence of oxygen atom might result from contamination of the ECR vacuum chamber, and/or surface contamination during the exposure of specimen in the open air [36,37]. The relative atomic concentration of carbon, nitrogen, and oxygen elements in the GNECN coating was calculated to be 82.6%, 13.8%, and 3.6%, respectively. The evolution of the nitrogen atomic concentration in the GNECN coating was presented with N/C atomic ratio, as shown in Table 2. It can be seen that the N/C atomic ratio increases from 0.17 to 0.25 with the increase of  $N_2/Ar$  ratio from 1/11 to 1/3. The maximum value of 0.25 was considerably lower than the theoretical value of 1.33 in the crystalline  $\beta$ - $C_3N_4$ . Hence, the carbon nitride in the GNECN coating remained an amorphous structure. Fig. 2 illustrates the HRTEM plan view image of GNECN coating fabricated at  $N_2/Ar$  ratio of 1/11. In comparison with the TEM images of the graphene sheets embedded carbon (GSEC) coatings prepared in our previous researches [27–32] together with the Raman spectra of the GNECN coatings (shown in Fig. 6), it can be seen that graphene nanocrystallites with a size of approximately 1–2 nm are randomly dispersed in the amorphous carbon nitride matrix. The distance between two graphene sheets is around 0.34 nm.

The effect of  $N_2/Ar$  ratio on the deposition rate, residual stress, surface roughness, and scratch depth of GNECN coatings is shown in Table 2. It was obviously observed that the deposition rate decreases greatly from 3.7 to 2.1 nm/min with increasing  $N_2/Ar$  ratio from 1/11 to 1/3. Similarly, the residual stress of GNECN coatings reduced gradually from 1.14 to 0.80 GPa with the increase of  $N_2/Ar$  ratio from 1/11

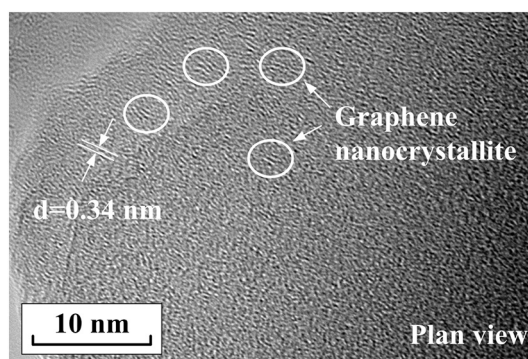


Fig. 2. A typical HRTEM plan view image of GNECN coating prepared at  $N_2/Ar$  ratio of 1/11.

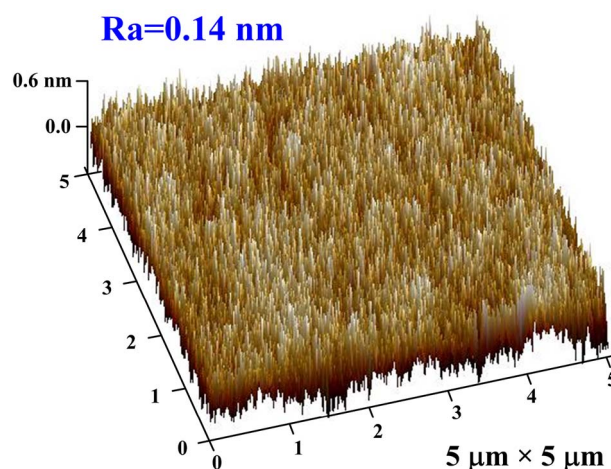


Fig. 3. AFM 3D image of GNECN coating prepared at  $N_2/Ar$  ratio of 1/3.

to 1/3. Fig. 3 shows a typical AFM 3D image of GNECN coating prepared at  $N_2/Ar$  ratio of 1/3. The arithmetic mean surface roughness (Ra) of the smooth GNECN coating was calculated to be 0.14 nm, slightly higher than the surface roughness of a polished Si substrate (around 0.08 nm). The surface roughness of GNECN coatings decreased from 0.22 to 0.14 nm with the increase of  $N_2/Ar$  ratio from 1/11 to 1/3. Fig. 4b presents a typical example of the cross-sectional topography across the scratch track (shown in Fig. 4a) of GNECN coating prepared at  $N_2/Ar$  ratio of 1/3 after the nanoscratch test. Consequently, the scratch depth of the GNECN coating was calculated to be 6.7 nm, more than twice of the scratch depth of Si substrate with a value of 2.7 nm. The scratch depth of GNECN coatings increased from 1.9 to 6.7 nm with the increase of  $N_2/Ar$  ratio from 1/11 to 1/3, suggesting a significant decrease of the nano-scratch resistance of the GNECN coatings.

To better understand the microstructural evolution as a function of  $N_2/Ar$  ratio and its correlation to the XPS and Raman spectra, GNECN coatings were analyzed with both XPS and Raman spectroscopy. Typical C1s and N1s core level spectra and the corresponding fitted Gaussian curves of GNECN coating prepared at  $N_2/Ar$  ratio of 1/11 are shown in Fig. 5a and b, respectively. The deconvoluted C1s spectrum consisted of three peaks located at binding energies of 284.7 eV, 285.5 eV, and 287.0 eV, which were attributed to  $sp^2$  C=C and C=N,  $sp^3$  C–C and C–N, and C–O bonds, respectively [38–40]. Whereas, the deconvoluted N1s spectrum consisted of four peaks located at binding energies of 398.2 eV, 399.4 eV, 400.7 eV, and 401.3 eV, which were attributed to  $sp^3$  C–N, C≡N,  $sp^2$  C=N, and N–O bonds, respectively [41–43]. The variation of C1s  $sp^3/sp^2$  and N1s  $sp^3/sp^2$  with  $N_2/Ar$  ratio is provided in Table 3. The percentage of  $sp^3$  bonding was slightly higher than that of  $sp^2$  bonding in the GNECN coatings. It was clearly shown that C1s  $sp^3/sp^2$  increases and N1s  $sp^3/sp^2$  decreases with the

Table 2

The N/C atomic ratio, deposition rate, residual stress, surface roughness, and scratch depth of GNECN coatings.

$N_2/Ar$ ratio	N/C atomic ratio	Deposition rate (nm/min)	Residual stress (GPa)	Surface roughness (nm)	Scratch depth (nm)
1/11	0.17	3.7	1.14	0.22	1.9
1/8	0.21	3.4	0.98	0.17	3.3
1/5	0.22	3.0	0.95	0.16	3.7
1/3	0.25	2.1	0.80	0.14	6.7

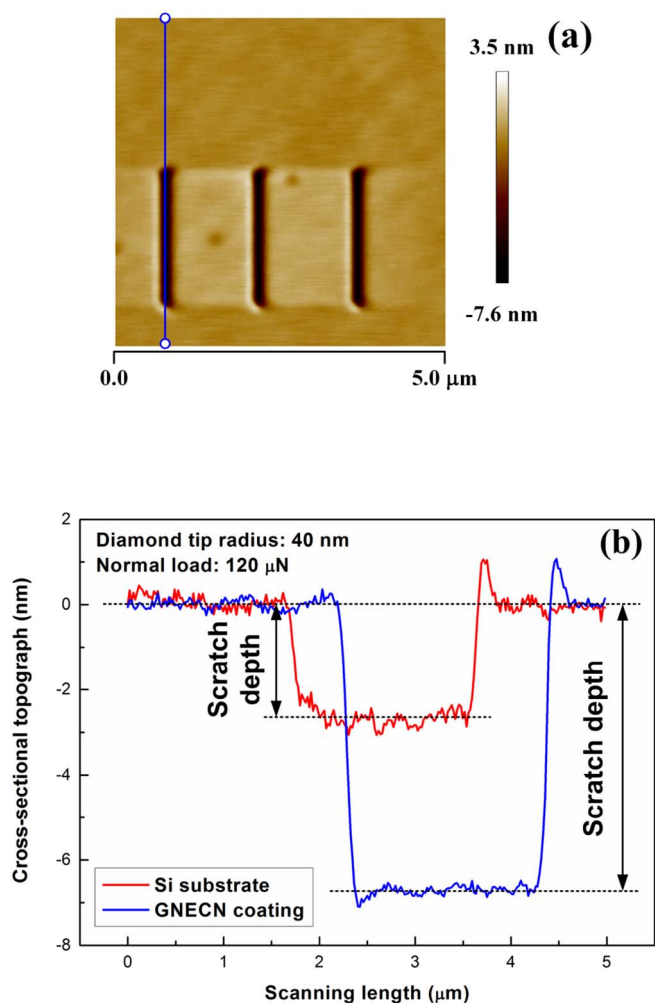


Fig. 4. (a) AFM 2D image of the scratch tracks and (b) cross-sectional topography across the scratch track of GNECN coating prepared at  $N_2/Ar$  ratio of 1/3. The scratch result of Si substrate is also shown for reference.

increasing  $N_2/Ar$  ratio from 1/11 to 1/3.

The Raman spectra and typical fitting curves of GNECN coatings are shown in Fig. 6. Each spectrum consisted of a D band and G band located at around  $1350$  and  $1590$   $cm^{-1}$ , respectively. Besides, a broad band located around  $2800$   $cm^{-1}$  instead of an individual 2D band was observed. The Raman spectrum ranging from  $900$  to  $1800$   $cm^{-1}$  was profile-fitted with a Lorentzian function for D peak located at Raman shift of around  $1350$   $cm^{-1}$ , a Breite-Wignere-Fano (BWF) function for G peak located at Raman shift of around  $1590$   $cm^{-1}$ , accompanied with a linear function for background subtraction [34,35]. The corresponding fitting results, such as D peak position, G peak position, and peak intensity ratio of D peak to G peak ( $I(D)/I(G)$ ) are listed in Table 3. Specifically, the shift of the D peak and G peak position could hardly be observed with the variation of  $N_2/Ar$  ratio. However, the  $I(D)/I(G)$  decreased from 1.29 to 1.07 with the increase of  $N_2/Ar$  ratio from 1/11 to 1/3, suggesting an increase of  $sp^3$  carbon bonding in the GNECN coatings. In summary of the Raman and XPS analyses, it was concluded that  $sp^3$  carbon bonding increases and  $sp^3$  nitrogen bonding decreases in the GNECN coatings with the increase of  $N_2/Ar$  ratio from 1/11 to 1/3.

In summary, graphene nanocrystallites with size of approximately 1–2 nm were successfully embedded into an amorphous carbon nitride matrix with the introduction of electron irradiation in an MCECR plasma sputtering system.  $N_2/Ar$  ratio was found to be an effective deposition parameter for tailoring the composition and structural

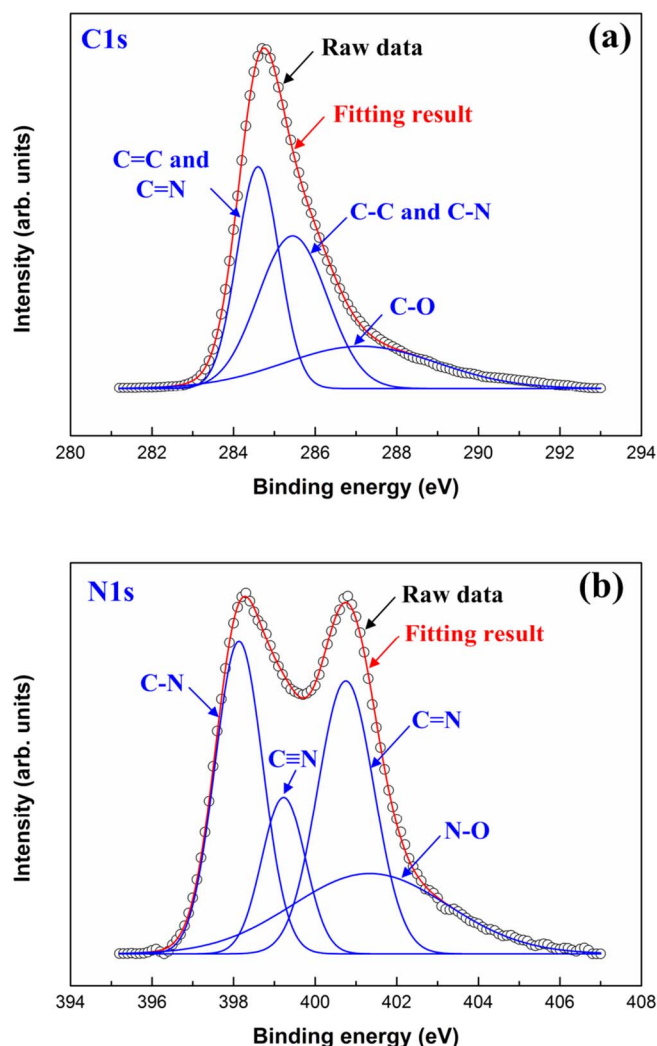


Fig. 5. Typical (a) C1s and (b) N1s core level spectra and the corresponding fitted Gaussian curves of GNECN coating prepared at  $N_2/Ar$  ratio of 1/11.

Table 3

The fitting results for XPS and Raman spectra of GNECN coatings.

$N_2/Ar$ ratio	C1s $sp^3/sp^2$	N1s $sp^3/sp^2$	D peak ( $cm^{-1}$ )	G peak ( $cm^{-1}$ )	$I(D)/I(G)$
1/11	0.91	1.23	1359	1595	1.29
1/8	1.09	1.09	1357	1590	1.17
1/5	1.02	1.11	1352	1588	1.07
1/3	1.12	0.97	1352	1590	1.07

properties of GNECN coatings, which is in good agreement with the previous studies [34,44,45]. On one hand, the increase of  $N_2/Ar$  ratio in the working gas generally leads to an increased deposition rate of graphite due to a higher sputtering yield of carbon by nitrogen compared with that of argon [34,46,47]. However, the re-sputtering and/or etching of the coating by nitrogen and argon ions in ECR plasma system was substantially stronger than those in CVD and PVD system, thus the maximum value of  $N_2/Ar$  ratio was limited to an extremely low value of 1/3 compared with 10 in a hybrid PVD-CVD system [34]. Therefore, the deposition rate of GNECN coatings decreased greatly with the increase of  $N_2/Ar$  ratio. Moreover, the increase of nitrogen species in the working gas caused higher incorporation of nitrogen atoms into the coatings, resulting in an increase of the N/C atomic ratio in GNECN coatings with the increase of  $N_2/Ar$  ratio. The increase in N/C atomic ratio caused a decreased residual stress, which is consistent with our

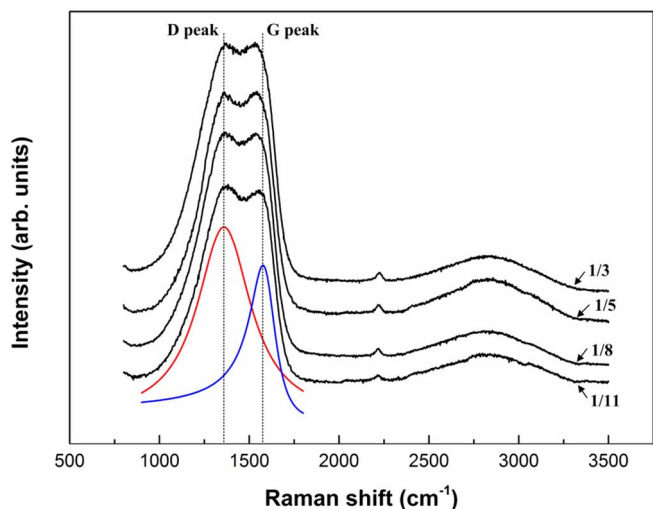


Fig. 6. Raman spectra and typical profile-fitting of Raman spectrum of GNECN coatings prepared at various  $N_2/Ar$  ratios.

previous studies [34,35]. Similarly, the surface roughness of GNECN coatings decreased due to the strong sputtering action under the impingement of nitrogen ions. Hence, a relatively smooth GNECN coating was obtained compared with a rough GSEC coating (e.g.  $R_a = 2\text{--}26\text{ nm}$  [27]) prepared with only argon plasma sputtering.

On the other hand, the increase of N/C atomic ratio in the GNECN coatings caused an increasing number of carbon  $sp^3$  bonding and a decreasing number of nitrogen  $sp^3$  bonding in a predominantly  $sp^3$  bonding structure. Hence, the incorporation of nitrogen atoms in the carbon structure was beneficial for the formation of  $sp^3$  bonding structure. The scratch depth of GNECN coatings increased with the increase of  $N_2/Ar$  ratio. Besides, the scratch depth of the GNECN coatings was remarkably lower than that of GSEC coatings (66.8 nm at normal load of 40  $\mu\text{N}$  [48]) with the introduction of nitrogen atoms. Therefore, it can be argued that the nano-scratch hardness of the GNECN coatings is mainly determined by the volume fraction of nitrogen  $sp^3$  bonding in the coating.

### 3.2. Tribological behavior of GNECN coatings

Fig. 7 shows representative friction curves of the GNECN coating prepared at  $N_2/Ar$  ratio of 1/11 as a function of sliding cycle when it runs against a  $Si_3N_4$  ball in ambient air and  $N_2$  gas stream. It was clearly

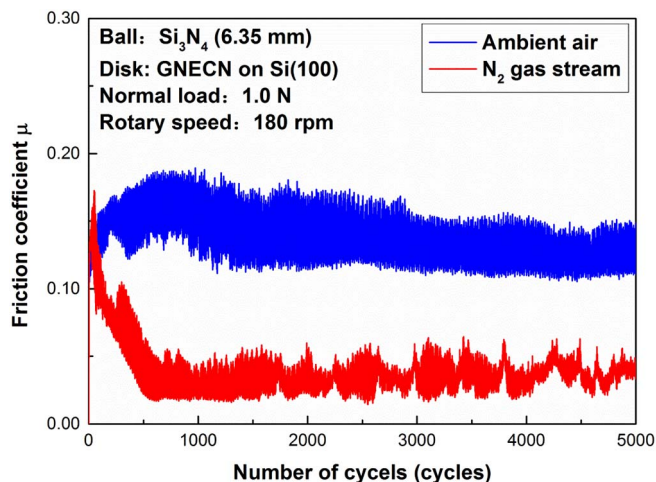


Fig. 7. Friction curves of GNECN coating prepared at  $N_2/Ar$  ratio of 1/11 when sliding against  $Si_3N_4$  ball in ambient air and  $N_2$  gas stream.

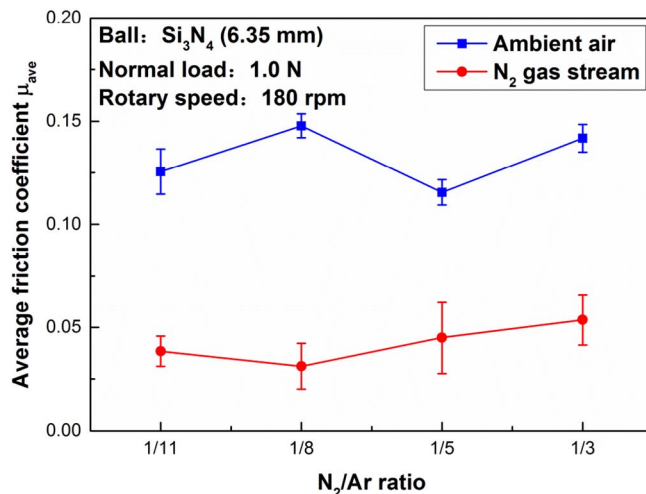


Fig. 8. Average friction coefficients of GNECN coatings prepared at various  $N_2/Ar$  ratios when sliding against  $Si_3N_4$  ball in ambient air and  $N_2$  gas stream.

observed that the friction coefficient in  $N_2$  gas stream is definitely lower than that in ambient air. Specifically, the friction coefficient in ambient air increased continuously from 0.10 to 0.15 after 1000 cycles, thereafter, the friction coefficient maintained a steady value of around 0.15. On the contrary, the friction coefficient in  $N_2$  gas stream decreased rapidly in the initial running-in stage for 500 cycles, and then it reached a relative stable value of lower than 0.05 (around one-third of the value observed in the ambient air) for the remainder of the sliding test. Similar friction behaviors were obtained for GNECN coatings prepared under other  $N_2/Ar$  ratios.

The average friction coefficients and corresponding standard deviations of GNECN coatings running against  $Si_3N_4$  balls both in ambient air and  $N_2$  gas stream are shown in Fig. 8. These values were evaluated by averaging the friction coefficients at the final 1000 cycles (i.e. 4000 to 5000 cycles) in each friction test. The average friction coefficients of GNECN coatings demonstrated less dependency on the  $N_2/Ar$  ratio. Specifically, they varied between 0.10 and 0.15 in ambient air and stabilized around 0.05 in  $N_2$  gas stream. The lowest and highest friction coefficients of  $0.031 \pm 0.011$  and  $0.148 \pm 0.006$  were obtained for the GNECN coating deposited at  $N_2/Ar$  ratio of 1/8 in  $N_2$  gas stream and ambient air, respectively.

To elucidate the low friction mechanisms of the GNECN coatings under  $N_2$  gas stream from the viewpoint of the composition and structural changes on the contact interfaces. The worn surfaces on both the  $Si_3N_4$  balls and the GNECN coated Si substrates after 5000 cycles sliding tests were observed and investigated by an optical microscope as well as Raman spectroscopy.

### 3.3. Structural changes on the worn surfaces

Optical images of worn surfaces on the  $Si_3N_4$  balls after running against the GNECN coatings prepared at various  $N_2/Ar$  ratios in ambient air and  $N_2$  gas stream are shown in Fig. 9a–d and e–h, respectively. It was shown that similar contact interfaces are obtained after friction tests in both ambient air and  $N_2$  gas stream except the wear scar on the  $Si_3N_4$  ball in Fig. 9a. Specifically, few tribofilms (visible transferred materials accumulated inside of the contact area) were observed on the wear scars of the ball surfaces after sliding tests in ambient air, as shown in Fig. 9b–d, whereas the wear scars of the ball surfaces were fully covered by large amount of tribofilms after sliding tests in  $N_2$  gas stream, as shown in Fig. 9e–h. The wear scar in Fig. 9a was an exception where a small amount of tribofilms were generated on the ball surface. It was proposed that low friction coefficients are attributed to the formation of the visible tribofilms on the  $Si_3N_4$  ball surfaces, whereas the

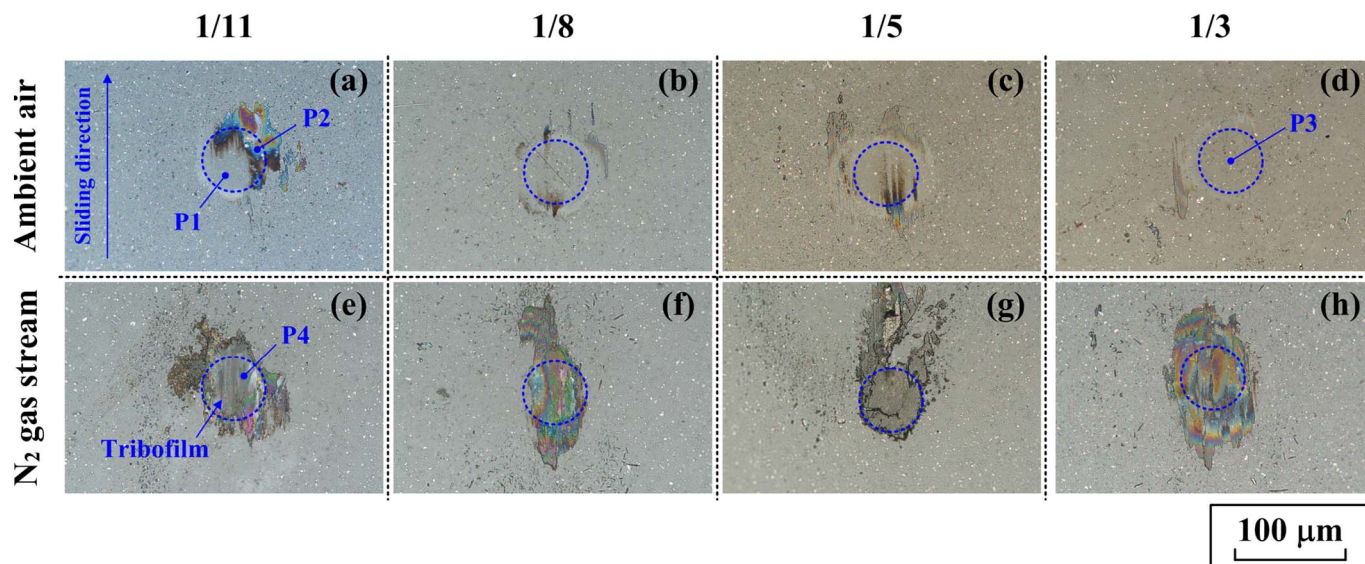


Fig. 9. Optical images of worn surfaces on the  $\text{Si}_3\text{N}_4$  ball after running against the GNECN coatings prepared at various  $\text{N}_2/\text{Ar}$  ratios in (a–d) ambient air and (e–h)  $\text{N}_2$  gas stream. The dotted circles indicate the theoretical contact area on the  $\text{Si}_3\text{N}_4$  ball surface. The sliding direction of the  $\text{Si}_3\text{N}_4$  ball is also shown for reference. The typical positions on worn surfaces for Raman analysis are marked with P1, P2, P3, and P4.

high friction coefficients are due to the direct sliding between the  $\text{Si}_3\text{N}_4$  balls and the GNECN coatings. Optical images of the GNECN coatings indicated similar contact interface and the coating did not wear out on the Si substrate surface after all the friction tests, and thus are not shown here.

To clarify the role of tribofilm on the wear scar of the ball surface in the low friction behavior of the GNECN coating, typical positions on the wear scars in Fig. 9 were studied with a Raman spectroscopy, as shown in Fig. 10a. In case of the high friction in ambient air, the Raman spectra of the tribofilm (P2) and no tribofilm (P1 and P3) were identical to the spectrum of the  $\text{Si}_3\text{N}_4$  ball with no specific peak, revealing no composition and structural changes on the ball surfaces in the high friction condition. On the other hand, the Raman spectrum of the tribofilm (P4) in  $\text{N}_2$  gas stream with low friction apparently consisted of two individual D and G peaks at Raman shifts of around  $1360\text{ cm}^{-1}$  and  $1590\text{ cm}^{-1}$ , respectively. The 2D peak located around  $2700\text{ cm}^{-1}$  could not be observed on the spectrum. The shift of G peak position to a higher value, which is considered as the formation of a graphitic or graphite-like structure [34,35,49], could not be identified. Supplementary Raman analyses of different positions (more than five places) on the tribofilms inside of the contact area on the  $\text{Si}_3\text{N}_4$  ball surface after sliding test in  $\text{N}_2$  gas stream showed similar results, suggesting a homogeneous tribofilm formed on the contact area of the ball surface in  $\text{N}_2$  gas stream.

Typical Raman spectra of worn surfaces on the GNECN coating prepared at  $\text{N}_2/\text{Ar}$  ratio of 1/8 after sliding against the  $\text{Si}_3\text{N}_4$  ball in ambient air and  $\text{N}_2$  gas stream, as shown in Fig. 10b, are similar to that of the as-deposited GNECN coating. However, the profile-fitting results of the Raman spectra definitely indicated that the value of  $I(\text{D})/I(\text{G})$  increases from the initial 1.17 in the as-deposited GNECN coating to 1.25 for the GNECN coating after friction test in  $\text{N}_2$  gas stream, and slightly decreased to 1.15 for the GNECN coating after friction test in ambient air. The increase of the  $I(\text{D})/I(\text{G})$  can be attributed to the formation of carbon  $\text{sp}^2$  structure (i.e. graphite-like structure) in the top surface, which is beneficial for achieving low friction coefficients of  $< 0.10$  of carbon-based coatings [13,50,51].

According to the Raman analyses of the  $\text{Si}_3\text{N}_4$  balls and the GNECN coatings, it was supposed that nano-size graphene structure is generated on the top surfaces of the contact interfaces after sliding tests in  $\text{N}_2$  gas stream in relation to the graphene nanocrystallites in the coatings. Raman spectra of the worn surfaces on the  $\text{Si}_3\text{N}_4$  ball and the GNECN

coating suggested that a homogeneous tribofilm together with the generation and evolution of the nano-size graphene structure are the key points in achieving stable and low friction coefficients of  $< 0.05$  of the GNECN coatings in  $\text{N}_2$  gas stream. Moreover, the high hardness of GNECN coating comparable to that of GSEC coating together with a similar interplanar spacing between graphene sheets strongly implied that the combination of low energy electron irradiation and nitrogen atom incorporation in the MCECR plasma sputtering system resulted in the embedding of soft graphene nanocrystallites into hard carbon nitride matrix, which is a beneficial architecture for obtaining stable and low friction coefficient in  $\text{N}_2$  gas stream. Nevertheless, the existence of nitrogen atoms in the GNECN coatings either in the form of amorphous carbon nitride matrix or in the form of nitrogen-doped graphene sheets can hardly be identified. However, experimental and first-principle simulation researches on the nitrogen-doped graphene have confirmed that the maximum nitrogen concentration in nitrogen-doped graphene material is limited to 5–6 at.% [52–55]. Therefore, it could be inferred that nitrogen atoms mainly exist in the amorphous carbon nitride matrix in the GNECN coatings. Further analyses of the nano- and micro-structure of the GNECN are highly required for thorough understanding of the low friction mechanisms in  $\text{N}_2$  gas stream. This research provides a way to develop nano-size crystallite embedded carbon nitride coatings with excellent mechanical and tribological performances for advanced engineering applications.

#### 4. Conclusions

Graphene nanocrystallite embedded carbon nitride (GNECN) coatings were fabricated on the silicon substrates using a MCECR plasma sputtering system working in an electron irradiation mode at various  $\text{N}_2/\text{Ar}$  ratios. The composition and structure of the GNECN coatings were closely related to the  $\text{N}_2/\text{Ar}$  ratio. It was clarified that the deposition rate, internal stress, and surface roughness of the GNECN coatings decrease whereas the N/C atomic ratio and scratch depth of the GNECN coatings increase with the increase of  $\text{N}_2/\text{Ar}$  ratio from 1/11 to 1/3. XPS and Raman analyses indicated an increasing number of carbon  $\text{sp}^3$  bonding and a decreasing number of nitrogen  $\text{sp}^3$  bonding in a predominant  $\text{sp}^3$  bonding structure in the GNECN coatings with the increasing  $\text{N}_2/\text{Ar}$  ratio. Graphene nanocrystallite was obviously identified in the amorphous carbon nitride structure from the analyses of TEM, XPS, and Raman spectroscopy. Most interestingly, the friction

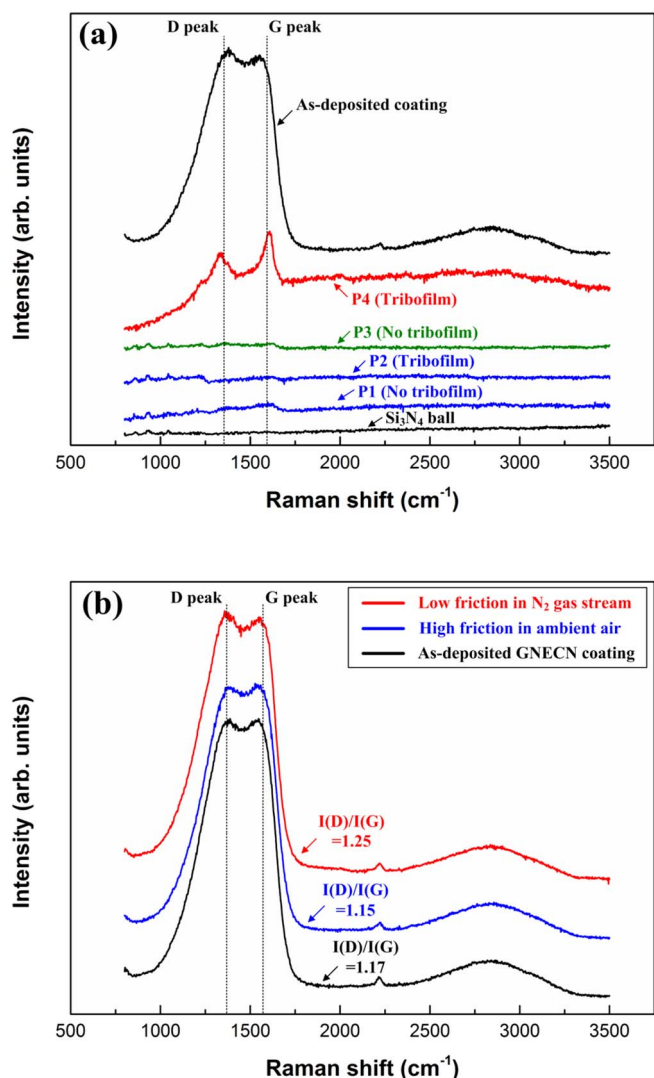


Fig. 10. Typical Raman spectra of worn surfaces on the (a)  $\text{Si}_3\text{N}_4$  balls and (b) the GNECN coatings after friction tests in ambient air and  $\text{N}_2$  gas stream. The spectrum of the as-deposited GNECN coating and the  $\text{Si}_3\text{N}_4$  ball is also shown for reference.

coefficients of the GNECN coatings showed less dependency on the  $\text{N}_2/\text{Ar}$  ratio, high friction coefficients ranging from 0.10 to 0.15 were obtained in ambient air, whereas, stable and low friction coefficients of  $< 0.05$  were achieved in  $\text{N}_2$  gas stream. The stable and low friction coefficients of GNECN coatings were attributed to the formation of a homogeneous tribofilm on the mating ball surface together with the generation and evolution of the nano-size graphene structure in the GNECN coating. It was strongly argued that the combination of low energy electron irradiation and nitrogen atom incorporation in the MCECR plasma sputtering system resulted in the embedding of soft graphene nanocrystallites into hard carbon nitride matrix, which is beneficial for obtaining stable and low friction coefficients of the GNECN coatings in  $\text{N}_2$  gas stream.

#### Conflict of interest

The authors declare no conflict of interest.

#### Acknowledgements

This work was supported by the National Nature Science Foundation of China with Grant Numbers of 51405308 and 51575359, Shenzhen Fundamental Research subject-layout project

(JCYJ20160427105015701), Natural Science Foundation of SZU (grant no. 827-000080), as well as the Young-Researcher-Starting grant of Shenzhen University (grant no. 201441). The authors thank Dr. Peidong Xue for his help in TEM observation.

#### References

- [1] A.Y. Liu, M.L. Cohen, Prediction of new low compressively solid, *Science* 245 (1989) 841–842.
- [2] N. Hellgren, M.P. Johansson, E. Broitman, L. Hultman, J.E. Sundgren, Role of nitrogen in the formation of hard and elastic  $\text{CN}_x$  thin films by reactive magnetron sputtering, *Phys. Rev. B* 59 (1999) 5162–5169.
- [3] R. Wäsche, M. Hartelt, U. Springborn, K. Bewilogua, M. Keuncke, Wear of carbon nitride coatings under oscillating sliding conditions, *Wear* 269 (2010) 816–825.
- [4] K.D. Bakoglidis, H. Glenat, G. Greczynski, S. Schmidt, S. Grillo, L. Hultman, E. Broitman, Comparative study of macro- and microtribological properties of carbon nitride thin films deposited by HiPIMS, *Wear* 370–371 (2017) 1–8.
- [5] M. Tsuchiya, K. Murakami, K. Magara, K. Nakamura, H. Ohashi, K. Tokuda, T. Takami, H. Ogasawara, Y. Enta, Y. Suzuki, S. Ando, H. Nakazawa, Structural and electrical properties and current–voltage characteristics of nitrogen-doped diamond-like carbon films on Si substrates by plasma-enhanced chemical vapor deposition, *Jpn. J. Appl. Phys.* 55 (2016) 065502.
- [6] C. Maddi, F. Bourquard, T. Tite, A.S. Loir, C. Donnet, F. Garrelie, V. Barnier, K. Wolski, P. Fortgang, N. Zehani, M. Braiek, F. Lagarde, C. Chaix, N. Jaffrezic-Renault, T.C. Rojas, J.C. Sánchez-López, Structure, electrochemical properties and functionalization of amorphous CN films deposited by femtosecond pulsed laser ablation, *Diam. Relat. Mater.* 65 (2016) 17–25.
- [7] H. Inoue, S. Muto, S. Arai, H. Wasada, N. Umehara, Microscopic origin of ultra-low friction coefficient between the wear track formed on carbon nitride coating and transfer layer on sliding ball in friction tests under dry  $\text{N}_2$ , *Surf. Coat. Technol.* 313 (2017) 31–39.
- [8] N. Yamada, T. Watari, T. Takeno, K. Adachi, Effect of oxygen on the self-formation of carbonaceous tribolayer with carbon nitride coatings under a nitrogen atmosphere, *Tribol. Lett.* 65 (2017) 27.
- [9] G. Goglio, D. Foy, G. Demazeau, State of art and recent trends in bulk carbon nitrides synthesis, *Mater. Sci. Eng. R* 58 (2008) 195–227.
- [10] P. Prieto, C. Quirós, E. Elizalde, A. Fernandez, J.M. Martin, J.M. Sanz, Carbon nitride films synthesized by dual ion beam sputtering, *Nucl. Instrum. Methods B* 122 (1997) 534–537.
- [11] J.C. Sánchez-López, M. Belin, C. Donnet, C. Quiros, E. Elizalde, Friction mechanisms of amorphous carbon nitride films under variable environments: a triboscopic study, *Surf. Coat. Technol.* 160 (2002) 138–144.
- [12] K. Kato, N. Umehara, K. Adachi, Friction, wear and  $\text{N}_2$ -lubrication of carbon nitride coatings: a review, *Wear* 254 (2003) 1062–1069.
- [13] P. Wang, M. Hirose, Y. Suzuki, K. Adachi, Carbon tribo-layer for super-low friction of amorphous carbon nitride coatings in inert gas environments, *Surf. Coat. Technol.* 221 (2013) 163–172.
- [14] P. Wang, K. Adachi, Low frictions of self-mated  $\text{CN}_x$  coatings in dry and humid inert gas environments, *Surf. Coat. Technol.* 258 (2014) 1137–1144.
- [15] P. Wang, M. Sugo, K. Adachi, Stable and super-low friction of amorphous carbon nitride coatings in nitrogen gas by using two-step ball-on-disk friction test, *Lubr. Sci.* 27 (2015) 137–149.
- [16] H. Sjöström, S. Stafström, M. Boman, J.E. Sundgren, Superhard and elastic carbon nitride thin films having fullerene-like microstructure, *Phys. Rev. Lett.* 75 (1995) 1336–1339.
- [17] T. Kamata, O. Niwa, S. Umemura, S. Hirono, The structure and bonding state for fullerene-like carbon nitride films with high hardness formed by electron cyclotron resonance plasma sputtering, *Jpn. J. Appl. Phys.* 51 (2012) 125602.
- [18] J. Bian, C. Huang, R.Q. Zhang, Graphitic carbon nitride film: an emerging star for catalytic and optoelectronic applications, *ChemSusChem* 9 (2016) 2723–2735.
- [19] J. Wen, J. Xie, X. Chen, X. Li, A review on g- $\text{C}_3\text{N}_4$ -based photocatalysts, *Appl. Surf. Sci.* 391 (2017) 72–123.
- [20] D. Berman, A. Erdemir, A.V. Sumant, Few layer graphene to reduce wear and friction on sliding steel surfaces, *Carbon* 54 (2013) 454–459.
- [21] D. Berman, A. Erdemir, A.V. Sumant, Graphene: a new emerging lubricant, *Mater. Today* 17 (2014) 31–42.
- [22] D. Berman, S.A. Deshmukh, S.K.R.S. Sankaranarayanan, A. Erdemir, A.V. Sumant, Macroscale superlubricity enabled by graphene nanoscroll formation, *Science* 348 (2015) 1118–1122.
- [23] X. Zheng, L. Gao, Q. Yao, Q. Li, M. Zhang, X. Xie, S. Qiao, G. Wang, T. Ma, Z. Di, J. Luo, X. Wang, Robust ultra-low-friction state of graphene via moiré superlattice confinement, *Nat. Commun.* 7 (2016) 13204.
- [24] S. Li, Q. Li, R.W. Carpick, P. Gumbsch, X.Z. Liu, X. Ding, J. Sun, J. Li, The evolving quality of frictional contact with graphene, *Nature* 539 (2016) 541–546.
- [25] S.W. Liu, H.P. Wang, Q. Xu, T.B. Ma, G. Yu, C. Zhang, D. Geng, Z. Yu, S. Zhang, W. Wang, Y.Z. Hu, H. Wang, J. Luo, Robust microscale superlubricity under high contact pressure enabled by graphene-coated microsphere, *Nat. Commun.* 8 (2017) 14029.
- [26] H. Song, L. Ji, H. Li, J. Wang, X. Liu, H. Zhou, J. Chen, Self-forming oriented layer slip and macroscale super-low friction of graphene, *Appl. Phys. Lett.* 110 (2017) 073101.
- [27] C. Chen, D. Diao, X. Fan, L. Yang, C. Wang, Frictional behavior of carbon film embedded with controlling-sized graphene nanocrystallites, *Tribol. Lett.* 55 (2014) 429–435.

- [28] C. Chen, X. Fan, D. Diao, Low-energy electron irradiation induced top-surface nanocrystallization of amorphous carbon film, *Appl. Surf. Sci.* 384 (2016) 341–347.
- [29] C. Wang, D. Diao, Cross-linked graphene layer embedded carbon film prepared using electron irradiation in ECR plasma sputtering, *Surf. Coat. Technol.* 206 (2011) 1899–1904.
- [30] C. Wang, D. Diao, X. Fan, C. Chen, Graphene sheets embedded carbon film prepared by electron irradiation in electron cyclotron resonance plasma, *Appl. Phys. Lett.* 100 (2012) 231909.
- [31] C. Wang, X. Zhang, D. Diao, Nanosized graphene crystallite induced strong magnetism in pure carbon films, *Nanoscale* 7 (2015) 4475–4481.
- [32] C. Wang, D. Diao, Self-magnetism induced large magnetoresistance at room temperature region in graphene nanocrystallized carbon film, *Carbon* 112 (2017) 162–168.
- [33] G.G. Stoney, The tension of metallic films deposited by electrolysis, *Proc. R. Soc. Lond. A* 82 (1909) 172–175.
- [34] P. Wang, T. Takeno, K. Adachi, H. Miki, T. Takagi, Preparation and tribological characterization of amorphous carbon nitride coatings in a RF PECVD–DC PVD hybrid coating process, *Appl. Surf. Sci.* 258 (2012) 6576–6582.
- [35] P. Wang, T. Takeno, J. Fontaine, M. Aono, K. Adachi, H. Miki, T. Takagi, Effects of substrate bias voltage and target sputtering power on the structural and tribological properties of carbon nitride coatings, *Mater. Chem. Phys.* 145 (2014) 434–440.
- [36] X. Yan, T. Xu, G. Chen, S. Yang, H. Liu, Q. Xue, Preparation and characterization of electrochemically deposited carbon nitride films on silicon substrate, *J. Phys. D: Appl. Phys.* 37 (2004) 907–913.
- [37] E. Ech-chamikh, A. Essafti, Y. Ijdiyaou, M. Azizan, XPS study of amorphous carbon nitride (a-C:N) thin films deposited by reactive RF sputtering, *Sol. Energy Mater. Sol. Cells* 90 (2006) 1420–1423.
- [38] H. Sjöström, L. Hultman, J.E. Sundgren, S.V. Hainsworth, T.F. Page, G.S.A.M. Theunissen, Structural and mechanical properties of carbon nitride  $CN_x$  ( $0.2 \leq x \leq 0.35$ ) films, *J. Vac. Sci. Technol. A* 14 (1996) 56–62.
- [39] F. Zhou, K. Adachi, K. Kato, Sliding friction and wear property of a-C and a- $CN_x$  coatings against SiC balls in water, *Thin Solid Films* 514 (2006) 231–239.
- [40] M. Aono, S. Aizawa, N. Kitazawa, Y. Watanabe, XPS study of carbon nitride films deposited by hot filament chemical vapor deposition using carbon filament, *Thin Solid Films* 516 (2008) 648–651.
- [41] S. Bhattacharyya, J. Hong, G. Turban, Determination of the structure of amorphous nitrogenated carbon films by combined Raman and X-ray photoemission spectroscopy, *J. Appl. Phys.* 83 (1998) 3917–3919.
- [42] Y.H. Cheng, X.L. Qiao, J.G. Chen, Y.P. Wu, C.S. Xie, S.B. Muo, Y.B. Sun, B.K. Tay, Synthesis of carbon nitride films by direct current plasma assisted pulsed laser deposition, *Appl. Phys. A Mater. Sci. Process.* 74 (2002) 225–231.
- [43] P. Gao, J. Xu, Y. Piao, W. Ding, X. Deng, C. Dong, Structure and tribology property of carbon nitride films deposited by MW-ECR plasma enhanced unbalanced magnetron sputtering, *Plasma Sci. Technol.* 8 (2006) 425–428.
- [44] H. Jung, H. Park, Correlation between deposition parameters and structural modification of amorphous carbon nitride (a- $CN_x$ ) film in magnetron sputtering, *Appl. Surf. Sci.* 216 (2003) 149–155.
- [45] Y.S. Zou, Q.M. Wang, H. Du, G.H. Song, J.Q. Xiao, J. Gong, C. Sun, L.S. Wen, Structural characterization of nitrogen doped diamond-like carbon films deposited by arc ion plating, *Appl. Surf. Sci.* 241 (2005) 295–302.
- [46] W.T. Zheng, H. Sjöström, I. Ivanov, K.Z. Xing, E. Broitman, W.R. Salaneck, J.E. Greene, J.E. Sundgren, Reactive magnetron sputter deposited  $CN_x$ : effects of  $N_2$  pressure and growth temperature on film composition, bonding, and microstructure, *J. Vac. Sci. Technol. A* 14 (1996) 2696–2701.
- [47] N. Nakayama, Y. Tsuchiya, S. Tamada, K. Kosuge, S. Nagata, K. Takahiro, S. Yamaguchi, Structural properties of amorphous carbon nitride films prepared by reactive RF-magnetron sputtering, *Jpn. J. Appl. Phys.* 32 (1993) L1465–L1468.
- [48] M. Guo, D. Diao, L. Yang, X. Fan, Restructured graphene sheets embedded carbon film by oxygen plasma etching and its tribological properties, *Appl. Surf. Sci.* 357 (2015) 771–776.
- [49] Y. Liu, A. Erdemir, E.I. Meletis, A study of the wear mechanism of diamond-like carbon films, *Surf. Coat. Technol.* 82 (1996) 48–56.
- [50] A. Erdemir, C. Donnet, Tribology of diamond-like carbon films: recent progress and future prospects, *J. Phys. D: Appl. Phys.* 39 (2006) R311–R327.
- [51] T. Tokoroyama, M. Kamiya, N. Umehara, C. Wang, D. Diao, Influence of UV irradiation in low frictional performance of  $CN_x$  coatings, *Lubr. Sci.* 24 (2012) 129–139.
- [52] D. Wei, Y. Liu, Y. Wang, H. Zhang, L. Huang, G. Yu, Synthesis of N-doped graphene by chemical vapor deposition and its electrical properties, *Nano Lett.* 9 (2009) 1752–1758.
- [53] L. Qu, Y. Liu, J.B. Baek, L. Dai, Nitrogen-doped graphene as efficient metal-free electrocatalyst for oxygen reduction in fuel cells, *ACS Nano* 4 (2010) 1321–1326.
- [54] C. Wang, Y. Zhou, L. He, T.W. Ng, G. Hong, Q.H. Wu, F. Gao, C.S. Lee, W. Zhang, In situ nitrogen-doped graphene grown from polydimethylsiloxane by plasma enhanced chemical vapor deposition, *Nanoscale* 5 (2013) 600–605.
- [55] X. Chen, D. He, S. Mu, Nitrogen-doped graphene, *Prog. Chem.* 25 (2013) 1292–1301.